On the evaluation of JRC effect on the shear strength of rock joints: reverse modelling of rock joints using a geo-statistical semivariogram model and 3d printing

Ghasem Shams & Patrice Rivard
Department of Civil Engineering – Université de Sherbrooke, Sherbrooke, Québec, Canada

ABSTRACT
Barton's criterion assumes that the rock joints with the same JRCs tested under the same conditions (same normal loading, same shear loading rate, etc.) have to result in the same shear strength. This paper aims at challenging this assumption. Reverse modeling of natural rock joints was applied to randomly generate the joint profiles with given JRCs (JRC 5 and 19) based on a previously developed statistical model. Then, a 3D printer was used to manufacture physical molds based on the morphology of generated joint profiles for casting mortar. Finally, direct shear tests were conducted in the lab on the cast mortar joint specimens with various surface morphologies. The experimental results indicated that the joint profiles with almost the same JRC values, but with different surface morphologies, lead to different shear strengths. It is concluded that the JRC might not appropriately represent the shear strength of rock joints, even for joints with the same properties.

RÉSUMÉ
Le critère de Barton suppose que les joints de roche avec les mêmes JRC testés dans les mêmes conditions (même charge normale, mêmes taux de charge de cisaillement, etc.) doivent avoir la même résistance au cisaillement. Cet article vise à remettre au défi cette hypothèse. La modélisation inverse des joints de roche naturelle a été appliquée pour générer de manière aléatoire les profils de joint avec des JRC donnés (JRC 5 et 19) sur la base d'un modèle statistique développé précédemment. Ensuite, une imprimante 3D a été utilisée pour fabriquer des moules physiques basés sur la morphologie des profils de joint générés pour couler le mortier. Enfin, des tests de cisaillement direct ont été réalisés en laboratoire sur des échantillons de joint de mortier coulé présentant diverses morphologies de surface. Les résultats expérimentaux ont indiqué que les profils de joint avec presque les mêmes valeurs JRC, mais avec des morphologies de surface différentes, conduisent à des résistances au cisaillement différentes. Il est conclu que le CCR pourrait ne pas représenter de manière appropriée la résistance au cisaillement des joints rocheux, même pour les joints ayant les mêmes propriétés.

1 INTRODUCTION

The most common approach for studying the shear strength of rock joints is performing the direct shear test under constant normal load/stress (CNL) in laboratory scale (Barton and Choubey 1977; Patton 1966; Tatone and Grasselli 2013; Yang et al. 2010; Zhang et al. 2016). However, such experimental tests require expensive equipment. Also, the sample preparation could be a complex and time-consuming procedure (Singh and Basu 2018). Hence, in an attempt to overcome these limitations, various empirical shear strength criteria have been proposed and employed to predict the shear strength of rock joints (Jaeger 1971; Kulatilake et al. 1995; Ladanyi and Archambault 1969; Patton 1966; Tatone and Grasselli 2009; Xia et al. 2014; Zhang et al. 2016).

Among the proposed criteria, the JRC-JCS model developed by Barton (1973) and Barton and Choubey (1977) (Eqs. 1 and 2, respectively) have been the most widely used shear constitutive model due to their simplicity and ease to predict the shear strength (Li and Zhang 2015; Singh and Basu 2018).

$$\tau = \sigma_n \left[\mathrm{JRC}. \log_{10} \left(\frac{\mathrm{JCS}}{\sigma_n} \right) + \varphi_b \right] \quad [1]$$

$$\tau = \sigma_n \left[\mathrm{JRC}. \log_{10} \left(\frac{\mathrm{JCS}}{\sigma_n} \right) + \varphi_r \right] \quad [1]$$

where τ is the peak shear strength, σ_n is the normal stress, JRC is the joint roughness coefficient, JCS is the strength of joint wall, φ_b is the basic friction angle, and φ_r is the residual friction angle.

Although Barton's model has significantly improved our understanding of rock joint behaviour, the reliability of this criterion is sometimes questionable in their application for predicting the shear strength of natural rock joints (Kulatilake et al. 1995; Zhao 1997; Wines and Lilly 2003; Du et al. 2011; Singh and Basu 2018). For instance, Kulatilake et al. (1995) stated that roughness profiles of rock joints consist of non-stationary and stationary components. According to them "the stationary profiles satisfy the following properties: (I) The mean surface is a constant with respect to the spatial location, (2) the variance of the surface height around the mean

surface is a constant with respect to the spatial location; and, (3) the covariance function of the surface height depends only on the lag distance, irrespective of the spatial location". However, as Kulatilake et al. (1995) pointed, in contrast to Barton's 10 standard profiles (Barton and Choubey 1977) that are stationary, most of the natural rock joint profiles do not satisfy all the above criteria, hence, are non-stationary. They stated that JRC cannot suitably represent this non-stationarity. Moreover, according to their experimental results, Kulatilake et al. (1995) concluded that Barton's criterion considerably underestimates the peak shear strength of rock joints, and there are significant differences between the experimental values and the values estimated by Barton's equation. In addition, Barton's JRC-JCS model is incompetent to capture the anisotropy of peak shear strength due to the anisotropy of joint surface roughness (Kulatilake et al. 1995). On the other hand, Zhao (1997) reported that Barton's JRC-JCS model overestimates the shear strength for natural joints with less matched surfaces. Furthermore, based on testing natural rock joints with mismatched surfaces, Du et al. (2011) noticed that there is an average relative error of 40% between the results obtained from laboratory direct shear tests and those predicted from the JRC-JCS empirical equation, indicating the incapability of Barton's JRC-JCS model to estimate joint shear strength for joints with less matched surfaces. Wines and Lilly (2003) also applied Barton's criterion to predict the shear strength of natural rock joints. The authors concluded that there is a significant discrepancy between the measured values from laboratory direct shear tests and the values estimated from Barton's JRC-JCS model. The experimental observations of Jiang et al. (2006) indicated that even though Barton's equation may be capable of predicting the shear strength of fairly smooth natural rock joints at low normal stresses, it tends to overpredict the shear strength for joints with very rough surfaces at a relatively high normal stress. Singh and Basu (2018) investigated the shear strength prediction efficiency of eleven shear strength criteria developed by various researchers including Barton's JRC-JCS model. After performing a total of 196 direct shear tests on natural joints of three distinct rock types, and comparing the measured shear strengths with the predicted ones, Singh and Basu (2018) reported that the shear strength criteria proposed by Barton (1973) resulted in an average error of 18.44 - 24.29% yielding a poor prediction performance.

Therefore, the aim of this study is to gain a better evaluation of the reliability of Barton's JRC-JCS model. For this purpose, several rock joint profiles with given JRC values were generated: 1) using digitalizing Barton's standard profiles, and 2) using a random generation method constructed on the basis of the two-dimensional geostatistics concept (Lê et al. 2018). Then, 3D printing technology was employed to build some molds based on the generated joint profiles for casting mortar specimens. Afterwards, laboratory direct shear tests were performed on the mortar cast joint specimens with different roughness characteristics to evaluate their shear behaviour.

2 METHODOLOGY

There are practical restrictions in providing natural rock joints with the same morphology for shear behaviour analysis. Therefore, researchers often use artificial rock joints generated by different methods, including 1) sawn joint surfaces cut by a disk-saw (Grasselli and Egger 2003; Jang et al. 2018), 2) artificial tensile joints produced by using Brazilian tests (Lee et al. 2001; Zhang et al. 2016; Zhao et al. 2018), and 3) cast natural or stylized joint surfaces with physical molds (Yang and Chiang 2000; Bahaaddini et al. 2016; Fathi et al. 2016). However, most of these methods are incapable to accurately reproduce natural rock joints with complicated and irregular surface morphologies. Moreover, the implementation of these methods is highly time-consuming (Jiang et al., 2016).

A promising alternative method for reproducing natural rock joints is the recently developed 3D printing (3DP) technology (Jiang and Zhao 2015; Jiang et al. 2016; Zhu et al. 2018). In this method, molds of joint surfaces with complicated morphologies can be generated quickly, with high accuracy up to a resolution of 10 microns. Complex structures can be manufactured in computer-aided design (CAD) and, then, be printed by a 3D printer (Sachs et al.1993).

In this study, 3D printing technique was applied to build several physical molds of rock joints with various surfaced morphology. These rock joint profiles were generated from 1) digitized profiles of Barton's standard joint roughness (JRC = 4 - 6, 10 - 12, and 18 - 20) (Nick Barton & Choubey, 1977), and 2) from 2D randomly generated profiles with corresponding JRCs (JRC = 5, 11, and 19) (Lê et al. 2018). The complete process of producing joint specimens is explained in following subsections.

2.1 Producing Rock Joint Profiles

2.1.1 Barton's Standard Joint Profiles

Two of Barton's standard joint profiles corresponding to JRC values of 4-6 and 18-20 were chosen to be used for mold production. The digitized x, y coordinates of both profiles were collected from the work conducted by Tatone (2009). These profiles were digitized with sampling intervals (SI) of 0.5 mm and are replotted in **Error! Reference source not found.**. The accuracy of the digitized profiles was evaluated and verified by Tatone (2009).

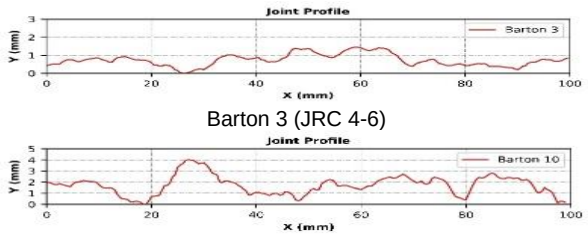

Figure 1. Two standard JRC profiles of Barton and Choubey (1977), digitized with horizontal sampling interval of 0.5 mm (Tatone, 2009).

2.1.2 Randomly-Generated Joint Profiles with a Particular JRC Value

Lê et al. (2018) performed a spatial statistical analysis on the 86 natural joint profiles including Barton's ten standard profiles and developed a new approach to estimate JRC. In their research, they digitized 86 joint profiles (all with a length of 10 cm) using a segment length of 0.25 mm (see Figure 2) and explored the relationship between the JRC and Profile Height Variation (PHV) by forming a semivariogram. The authors defined PHV as the height difference between any two adjacent points (separated by 0.25 mm) on a digitized profile (Figure 2). Their analysis indicated that there is a strong dependency between the standard deviation of the PHV and the JRC value. The results of their statistical analysis also showed that for different JRC values, the PHV follows a normal distribution, with an average of zero and a standard deviation that is a function of the JRC value. Indeed, they proposed an empirical equation that relates the standard deviation of the PHV of a joint surface to its JRC value (Eq. 3).

Therefore, they claimed that based on the statistical characteristics of the PHV, any random profile with a given JRC can be produced for further analysis.

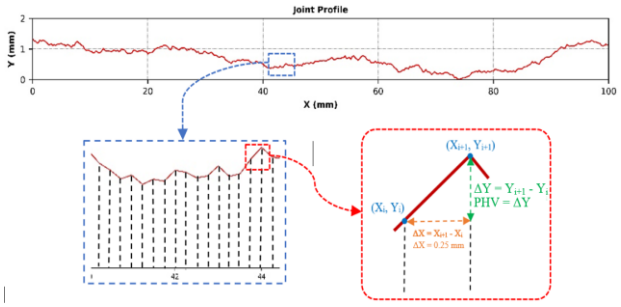

Figure 2. PHV (ΔY) calculation (Lê et al., 2018).

$$\text{Standar Deviation of PHV} = 0.0277e^{0.0687JRC} \quad [2]$$

In this study, the PHV method was applied to randomly generate joint profiles with JRC values of 5, 11, and 19 corresponding to Barton's profiles of 4-6, 10-12, and 18-20, respectively. Accordingly, for producing a joint profile with a length of 10 cm, 399 PHVs (separated by 0.25 mm) were generated following a normal distribution with a zero mean and a JRC-related standard deviation of the PHV (Eq. 3). The joint profile was finally constructed by summing the 399 PHVs and assuming that the joint profile starts at a zero elevation (Lê et al., 2018).

Figure 3 shows the randomly generated profiles with JRCs of 5 and 19. Note that three different joint profiles were generated for each given JRC. To evaluate the performance of the PHV method, JRC values of the generated profiles was re-calculated using Eqs. 4 and 5 for each joint profile as shown in Table 1 (Li and Zhang 2015; Yu and Vayssade, 1991):

$$\text{JRC} = 56.15 \times \sqrt{Z_2} - 16.99 \quad [3]$$

$$\text{JRC} = 28.10 \times \log(Z_2) + 28.43 \quad [4]$$

where Z_2 is the root mean square of the first deviation of the joint profile, which is given by Eq. 6 (Myers 1962).

$$Z_2 = \left[\frac{1}{L}\int_{x=0}^{x=L}\left(\frac{dy}{dx}\right)^2 dx\right]^{1/2} = \left[\frac{1}{L}\sum_{i=1}^{n-1}\frac{(y_{i+1}-y_i)^2}{x_{i+1}-x_i}\right]^{1/2} \quad [5]$$

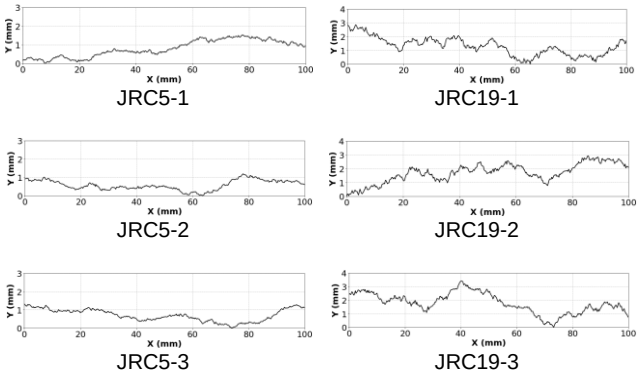

Figure 3. Randomly generated joint profiles with JRC 5 (1, 2, 3) and JRC 19 (1, 2, 3).

Table 1 : Verification of randomly generated profiles using empirical equations

Given JRC	Profile No.	Z_2^*	Estimated JRC	Estimated JRC (Average)	Error (%)
JRC = 5	JRC 5-1	0.153	4.95 [4] 5.50 [5]	5.22	4.46
	JRC 5-2	0.156	5.18 [4] 5.75 [5]	5.47	9.44
	JRC 5-3	0.149	4.62 [4] 5.13 [5]	4.88	-2.43
JRC = 19	JRC 19-1	0.436	20.09 [4] 18.30 [5]	19.19	1.01
	JRC 19-2	0.426	19.65 [4] 18.00 [5]	18.82	-0.91
	JRC 19-3	0.420	19.39 [4] 17.83 [5]	18.61	-2.03

*Z_2 was calculated with sampling intervals of (SI) 0.25 mm.

2.2 3D Printer-Manufactured Joint Specimens

After generating the virtual rock joint profiles, physical molds were produced using a Ultimaker-3 3D printer (Cura 2018). In brief, printing a 3D object is fulfilled in 3 steps (Berman, 2012; Saxena, 2016): 1) produce a virtual 3D model using computer-aided design (CAD) software, 2) convert CAD drawing files to the STL format, and 3) upload STL files to a 3D printer and build the physical molds. The length and the width of the rock joint specimens were designed to be 100 and 90 mm, respectively, to comply with the shear test machine. Figure 4 depicts an example of a printed joint surface.

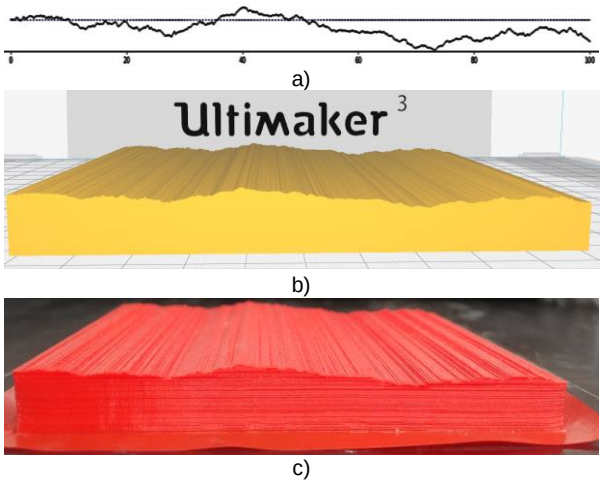

a) b) c)

Figure 4. Example of a printed joint model including a) the randomly generated profile for JRC 19, b) the STL file uploded to 3D printer, and c) the manufactured mold.

2.3 Replication of the Joint Specimens

The process of specimen replication can be explained as follows:

I. The 3D printer-built joint specimens were installed inside a PVC box for mortar casting (Figure 5a). In this step, the lower-half of each joint model was replicated (Figure 5b).

II. After 24 hours, the lower-half of the specimen and the mold were detached from the box. The lower semi-sample was then kept in the water and in a room of a temperature at 90° for a curing time of 48 hours. Afterwards, it was put in water for 5 days in room temperature.

III. The cast lower-half block is placed in the PVC box and mortar is grouted into the box. After 24 hours, the upper-half of the joint model is set and ready to be detached from the box (Figure 5c).

IV. The step ii is repeated for the upper semi-sample.

The material used for creating the joint models is a high-performance mortar with an average unconfined compressive strength (UCS) of 171 MPa after 8 days of curing.

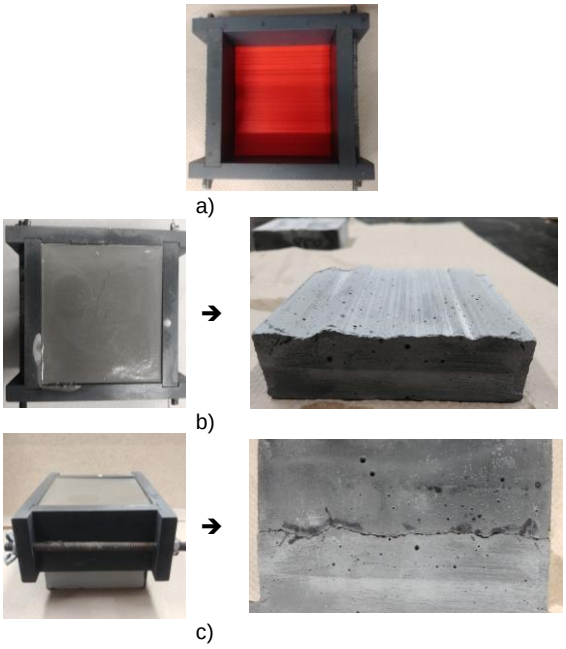

a) b) c)

Figure 5. Producing mortar specimens: (a) installing the printed mold, (b) casting the lower semi-block, (c) casting the upper semi-block directly on the pre-cast lower semi-block.

The joint surface of the mortar specimens was scanned using a profilometer laser scanner (Kreon Zephyr© 25). Afterwards, the 2D profiles of the scanned surfaces were compared with the corresponding profiles of the original joint models (Table 2).

Table 2. Z_2 values for the original joint profiles and the 2D profiles of the cast mortar specimens.

Profile no.	Z_2			Error (%)
	Sampling Interval	Original Profiles	Mortar Profiles	
JRC 5-1	0.25	0.153	0.147	3.73
JRC 5-2	0.25	0.156	0.154	1.28
JRC 5-3	0.25	0.149	0.145	2.16
JRC 11-1	0.25	0.237	0.236	0.42
JRC 11-2	0.25	0.238	0.236	0.84
JRC 11-3	0.25	0.240	0.234	2.34
JRC 19-1	0.25	0.436	0.422	3.21
JRC 19-2	0.25	0.426	0.425	0.16
JRC 19-3	0.25	0.420	0.403	4.00
Barton 3	0.5	0.128	0.124	3.11
Barton 6	0.5	0.213	0.210	1.55
Barton 10	0.5	0.394	0.380	3.65

The small error values in Table 2 indicates that natural rock joints with various surface morphologies and with different JRC values can be fabricated by using the 3DP technology with a high accuracy. Note that the Z_2 values in Table 2 were calculated with sampling intervals of 0.25 and 0.5 mm for randomly generated profiles (Lê et al. 2018) and Barton's profiles (Tatone, 2009), respectively.

Furthermore, through calculating the Z_2 parameter, a quantitative comparison was also made between the cast mortar joints and the original profiles (Figure 6).

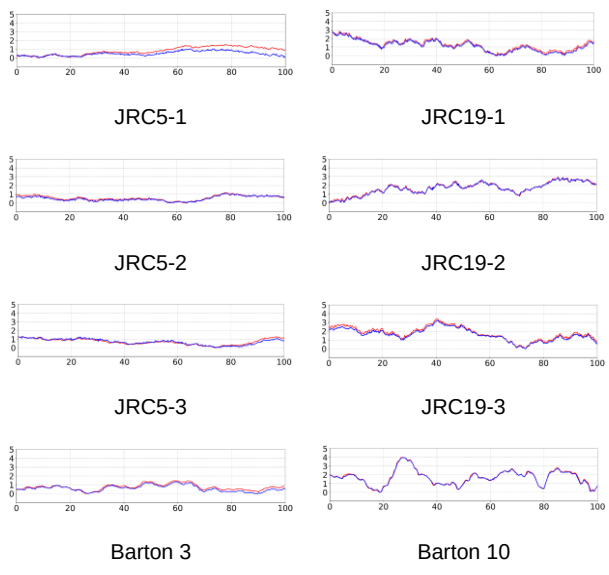

Figure 6. Comparison of the joint profiles between the 2D profiles of the scanned surfaces (blue) and their corresponding original joint profiles (red)

3 DIRECT SHEAR TEST RESULTS AND DISCUSSION

Eight direct shear tests were performed under a normal stress of 0.2 MPa. The shear stress and dilation versus shear displacement for joints with JRC 5 and 19 are shown in Figures 7 and 8, respectively.

As Figure 7 displays, all joint samples with JRC 5 exhibit a lower peak shear stress compared to that of the Barton-3 sample. The shear strengths of JRC5-1, JRC5-2, JRC5-3, and Barton-3 are 0.28, 0.26, 0.28, 0.32 MPa, respectively. Furthermore, the dilation value for Barton-3 joint sample is much higher (more than 3.5 times after 3 mm shear displacement) than those of the 3D printer-built joint specimens.

Similarly, as illustrated in **Error! Reference source not found.**, all joint samples with JRC 19 present a lower shear strength compared to the Barton-10 sample. The shear strengths of JRC19-1, JRC19-2, JRC19-3, and Barton-10 are 0.27, 0.20, 0.39, 0.89 MPa, respectively. It is important to note that the difference between the shear strength of samples with JRC 19 and Barton-10 (maximum 0.69 MPa) is much higher than this difference between specimens with JRC 5 and Barton-3 (maximum 0.06 MPa). **Error! Reference source not found.** also points out that the 3D printer-built joint specimens resulted in approximately the same dilation values, which are again less than Barton-10's dilation.

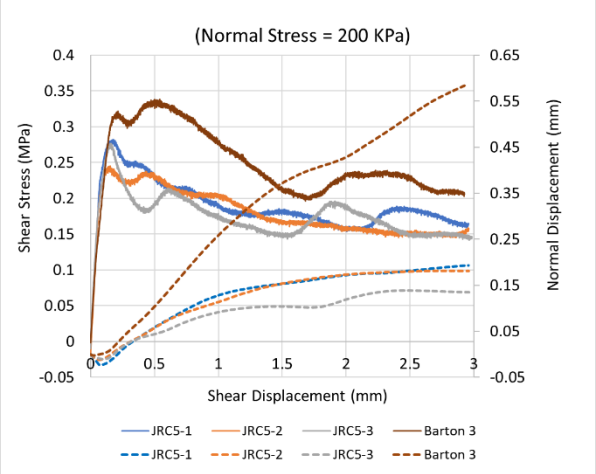

Figure 7. Shear stress–shear displacement (solid lines) and normal displacement–shear displacement (dash lines) for rock joint samples with JRC 5.

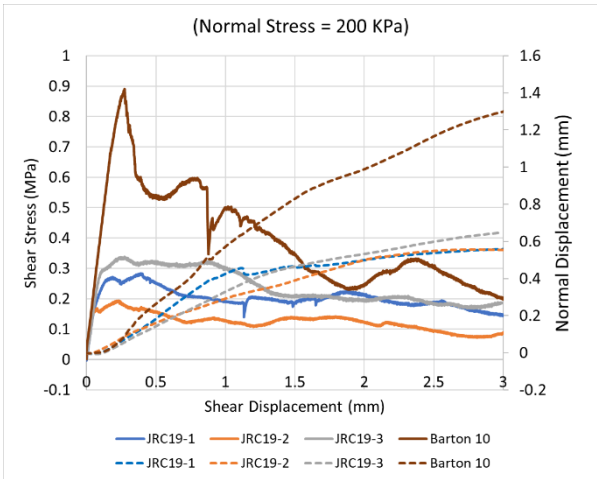

Figure 8. Shear stress–shear displacement (solid lines) and normal displacement–shear displacement (dash lines) for rock joint samples with JRC 19.

To better explain the obtained experimental results, all curves are re-plotted together in Figures 9 and 10. As seen in Figure 9, regardless of Barton-10, which has the highest shear strength, Barton-3 has a shear strength that is roughly similar to the shear strength of the profiles with JRC-19 and JRC-5. On the other hand, Figure 10 clearly indicates that the dilation in all cases shows similar results for the profiles generated by 3D printing. While all JRC-5 joint profiles have a dilation below 0.2 mm after 3 mm of shear displacement, dilation for JRC-19 samples is around 0.6 mm.

Based on the joint profiles shown in Figures 1 and 3 and the dilation curves depicted in Figure 10, it can be inferred that, at low levels of normal stress, the dilation is controlled by the primary “large-scale” asperities (the bumps at the joint surface). Although the randomly generated profiles have JRC values of 19, in terms of the primary asperities, these profiles are smoother than Barton's profile with a JRC of 18–20. Therefore, Barton’s profiles are more dilatant than the randomly generated profiles; for instance, the Barton-3 joint profile shows a dilatation value equivalent to those of JRC-19 samples.

Regarding the shear strength, no clear explanation could be drawn about the effect of roughness on the peak shear strength. However, it appears that the primary asperities also govern the shear strength of the tested samples. When the amplitude of the primary asperities is large, and the asperities are steep like Barton-10 and JRC19-3, the secondary asperities have a negligible effect on the shear strength. For example, among all joint models that were investigated here, Barton-10 sample exhibits the primary asperities with largest amplitude; it resulted in the highest shear strength. Besides, the Barton-3 joint profile and JRC19-3 have primary bumps with similar amplitude, and therefore, similar shear strength. However, the JRC19-3 profile has much more secondary asperities appeared on those primary asperity, and therefore, has a much higher JRC value than Barton-3. Samples JRC5-1, JRC5-2, JRC5-3, JRC19-1, and JRC19-2 have primary asperities with nearly similar amplitudes, and hence, similar shear strengths.

Moreover, another factor that may affect the shear strength is the distribution of primary and secondary asperities along the joint profiles (especially for those joints composed of primary asperities with small amplitudes). For instance, for the JRC5-1, JRC5-2, JRC5-3 joint samples, the primary asperities have a more uniform distribution along their profiles. This uniformity in the primary asperities distribution may result in a more uniform stress distribution (i.e. less stress concentration) along the joint surfaces. In such circumstances, the secondary asperities may fail under higher shear stress values, which would result in higher shear strength. On the contrary, non-uniform distribution of the primary asperities along the JRC19-2 sample might have produced high stress concentrations, and thus, imposed a failure of micro-asperities at lower levels of shear stress.

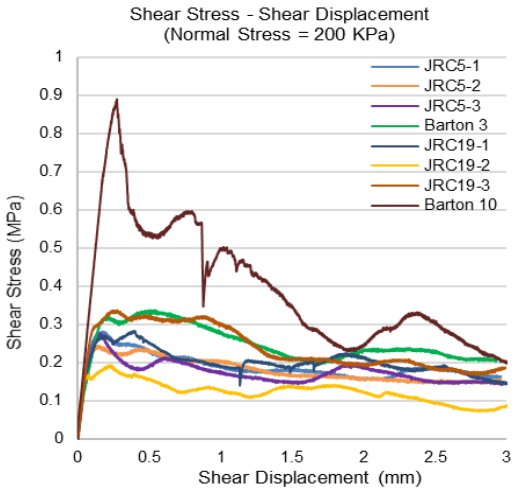

Figure 9. Shear stress–shear displacement for rock joint samples with JRC values of 5 and 19.

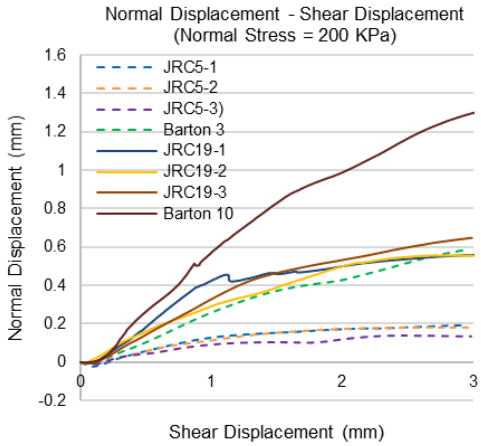

Figure 10. Normal displacement – shear displacement showing dilation for rock joint samples with JRC 5 and 19.

4 CONCLUSIONS

A series of joint profiles with different JRC values were generated by digitizing Barton's standard profiles and applying a statistical method. 3D printing technology was then applied to build physical molds with different surface morphologies for casting mortar. The joint surfaces of the mortar specimens were scanned and compared with the corresponding profiles of the original joint models. The comparison confirmed the reliability of the used approach for generating rock joints with various JRCs.

Direct shear tests of the joint profiles were performed. The experimental results indicated that even for joints with JRC value of 19 the shear strength may be lower than that of those joints with lower JRC values. The results indicate that at low levels of normal stress it is mainly the primary asperities that control both the shear strength and the dilatancy of rock joints.

It should be noted that although all JRC-19 joint profiles are visually rougher than the JRC-5 joint profiles due to the appearance of the secondary asperity, they all have primary asperities with almost similar amplitudes. And while the entire roughness of these profiles is composed of both the primary and secondary asperities, and the micro-asperities highly contribute to the calculation of JRC values, they have minor effect on the shear behaviour of rock joints. As a result, the question is that if JRC is a reliable and appropriate parameter for predicting the shear strength of natural rock joints in any case. Many researchers have reported that JRC does not always lead to satisfactory estimation of the shear strength of natural rock joints (Jiang et al. 2006; Singh and Basu 2018; Zhao 1997).

5 REFERENCES

Alejano, L. R., González, J. and Muralha, J. 2012. Comparison of different techniques of tilt testing and basic friction angle variability assessment, *Rock Mechanics and Rock Engineering*, 45(6): 1023–1035.

Bahaaddini, M., Hagan, P. C., Mitra, R. and Khosravi, M. H. 2016. Experimental and numerical study of asperity degradation in the direct shear test, *Engineering Geology*, 204: 41–52.

Bandis, S. 1980. *Experimental studies of scale effects on shear strength, and deformation of rock joints*, Doctoral dissertation, University of Leeds.

Barton, N. 1973. Review of a new shear-strength criterion for rock joints, *Engineering Geology*, 7(4): 287–332.

Barton, N. and Choubey, V. 1977. The shear strength of rock joints in theory and practice, *Rock Mechanics*, 10(1–2): 1–54.

Berman, B. 2012. 3-D printing: The new industrial revolution, *Business Horizons*, 55(2): 155–162.

Bruce, I. G., Cruden, D. M. and Eaton, T. M. 1989. Use of a tilting table to determine the basic friction angle of hard rock samples, *Canadian Geotechnical Journal*, 26(3): 474–479.

Cura, U. 2018. Online: https://ultimaker.com/en/products/ultimaker-3.

Du, S., Hu, Y., Hu, X. and Guo, X. 2011. Comparison between empirical estimation by JRC-JCS model and direct shear test for joint shear strength, *Journal of Earth Science*, 22(3): 411–420.

Fathi, A., Moradian, Z., Rivard, P., Ballivy, G. and Boyd, A. J. 2016. Geometric Effect of Asperities on Shear Mechanism of Rock Joints. *Rock Mechanics and Rock Engineering*, 49(3): 801–820.

Geertsema, A. J. 2002. The shear strength of planar joints in mudstone, *International Journal of Rock Mechanics and Mining Sciences,* 8(39): 1045–1049.

Grasselli, G. and Egger, P. 2003. Constitutive law for the shear strength of rock joints based on three-dimensional surface parameters, *International Journal of Rock Mechanics and Mining Sciences*, 40(1): 25–40.

Jaeger, J. C. 1971. Friction of Rocks and Stability of Rock Slopes, *Géotechnique*, 21(2): 97–134.

Jang, H. S., Zhang, Q. Z., Kang, S. S. and Jang, B. A. 2018. Determination of the Basic Friction Angle of Rock Surfaces by Tilt Tests, *Rock Mechanics and Rock Engineering*, 51(4): 989–1004.

Jiang, C. and Zhao, G.-F. 2015. A preliminary study of 3D printing on rock mechanics, *Rock Mechanics and Rock Engineering*, 48(3): 1041–1050.

Jiang, Q., Feng, X., Gong, Y., Song, L., Ran, S. and Cui, J. 2016. Reverse modelling of natural rock joints using 3D scanning and 3D printing, *Computers and Geotechnics*, 73: 210–220.

Jiang, Y., Li, B. and Tanabashi, Y. 2006. Estimating the relation between surface roughness and mechanical properties of rock joints, *International Journal of Rock Mechanics and Mining Sciences*, 43(6): 837–846.

Kulatilake, P. H. S. W., Shou, G., Huang, T. H. and Morgan, R. M. 1995. New peak shear strength criteria for anisotropic rock joints, *International Journal of Rock Mechanics and Mining Sciences & Geomechanics Abstracts*, 32(7): 673–697.

Kumar, R. and Verma, A. K. 2016. Anisotropic shear behavior of rock joint replicas, *International Journal of Rock Mechanics and Mining Sciences*, 90: 62–73.

Ladanyi, B. and Archambault, G. 1969. Simulation of shear behavior of jointed rock mass, *the 11th U.S. Symposium on Rock Mechanics (USRMS),* American Rock Mechanics Association, 105–125.

Lê, H. K., Huang, W.-C., Liao, M.-C. and Weng, M.-C. 2018. Spatial characteristics of rock joint profile roughness and mechanical behavior of a randomly generated rock joint, *Engineering Geology*, 245(January): 97–105.

Lee, H. S., Park, Y. J., Cho, T. F. and You, K. H. 2001. Influence of asperity degradation on the mechanical behavior of rough rock joints under cyclic shear loading, *International Journal of Rock Mechanics and Mining Sciences*, 38(7): 967–980.

Li, Y., Oh, J., Mitra, R. and Hebblewhite, B. 2016. A constitutive model for a laboratory rock joint with multi-scale asperity degradation, *Computers and Geotechnics*, 72: 143–151.

Li, Y. and Zhang, Y. 2015. Quantitative estimation of joint roughness coefficient using statistical parameters, *International Journal of Rock Mechanics and Mining Sciences*, 77: 27–35.

Myers, N. O. 1962. Characterization of surface roughness, *Wear*, 5(3): 182–189.

Patton, F. D. 1966. Multiple modes of shear failure in rock, *1st ISRM Congress*, International Society for Rock Mechanics and Rock Engineering.

Sachs, E. M., Haggerty, J. S., Cima, M. J. and Williams, P. A. 1993. *Three-dimensional printing techniques,* U.S. Patent No. 5,204,055.

Saxena, A. 2016. A Comprehensive Study on 3D Printing Technology, 3D Printing Technology, *MIT Int J Mech Eng.*, 6(2): 63-69..

Singh, H. K. and Basu, A. 2018. Evaluation of existing criteria in estimating shear strength of natural rock discontinuities, *Engineering Geology,* 232, 171–181.

Song, L., Jiang, Q., Shi, Y.-E., Feng, X.-T., Li, Y., Su, F. and Liu, C. 2018. Feasibility investigation of 3D printing technology for geotechnical physical models: study of tunnels, *Rock Mechanics and Rock Engineering*, 51(8): 2617–2637.

Sow, D., Rivard, P., Peyras, L., Breul, P., Moradian, Z. A., Bacconnet, C. and Ballivy, G. 2016. Comparison of Joint Shearing Resistance Obtained with the Barton and Choubey Criterion and with Direct Shear Tests, *Rock Mechanics and Rock Engineering*, 49(8): 3357–3361.

Tang, Z. C. and Wong, L. N. Y. 2016. New criterion for evaluating the peak shear strength of rock joints under different contact states, *Rock Mechanics and Rock Engineering*, 49(4): 1191–1199.

Tatone, B. S. A. 2009. *Quantitative characterization of natural rock discontinuity roughness in-situ and in the laboratory*, Doctoral Dissertation, University of Toronto, Toronto, Canada.

Tatone, B. S. A. and Grasselli, G. 2009. A method to evaluate the three-dimensional roughness of fracture surfaces in brittle geomaterials, *Review of Scientific Instruments*, 80(12): 125110.

Tatone, B. S. A. and Grasselli, G. 2013. An investigation of discontinuity roughness scale dependency using high-resolution surface measurements, *Rock Mechanics and Rock Engineering*, 46(4): 657–681.

Wines, D. R. and Lilly, P. A. 2003. Estimates of rock joint shear strength in part of the Fimiston open pit operation in Western Australia, *International Journal of Rock Mechanics and Mining Sciences*, 40(6): 929–937.

Xia, C. C., Tang, Z. C., Xiao, W. M. and Song, Y. L. 2014. New peak shear strength criterion of rock joints based on quantified surface description, *Rock Mechanics and Rock Engineering*, 47(2): 387–400.

Yang, Z.-Y., Taghichian, A. and Li, W.-C. 2010. Effect of asperity order on the shear response of three-dimensional joints by focusing on damage area, *International Journal of Rock Mechanics and Mining Sciences*, 6(47): 1012–1026.

Yang, Z. Y. and Chiang, D. Y. 2000. An experimental study on the progressive shear behavior of rock joints with tooth-shaped asperities, *International Journal of Rock Mechanics and Mining Sciences*, 37(8): 1247–1259.

Yu, X. and Vayssade, B. 1991. Joint profiles and their roughness parameters, *International Journal of Rock Mechanics and Mining Sciences and geomechanics abstracts*, 28(4): 333–336.

Zhang, X., Jiang, Q., Chen, N., Wei, W. and Feng, X. 2016. Laboratory Investigation on Shear Behavior of Rock Joints and a New Peak Shear Strength Criterion, *Rock Mechanics and Rock Engineering*, 49(9): 3495–3512.

Zhao, J. 1997. Joint surface matching and shear strength part B: JRC-JMC shear strength criterion, *International Journal of Rock Mechanics and Mining Sciences*, 34(2): 179–185.

Zhao, Z., Peng, H., Wu, W. and Chen, Y. F. 2018. Characteristics of shear-induced asperity degradation of rock fractures and implications for solute retardation, *International Journal of Rock Mechanics and Mining Sciences*, 105(March): 53–61.

Zhu, J. B., Zhou, T., Liao, Z. Y., Sun, L., Li, X. B. and Chen, R. 2018. Replication of internal defects and investigation of mechanical and fracture behaviour of rock using 3D printing and 3D numerical methods in combination with X-ray computerized tomography, *International Journal of Rock Mechanics and Mining Sciences*, 106(February): 198–212.